Electroencephalography and clinical Neurophysiology, 1986, 65: 344–360
Elsevier Scientific Publishers Ireland, Ltd.

EVOKED DIPOLE SOURCE POTENTIALS OF THE HUMAN AUDITORY CORTEX

MICHAEL SCHERG [1] and DETLEV VON CRAMON

Max Planck Institute for Psychiatry, Department of Neuropsychology, D-8000 Munich 40 (F.R.G.)

(Accepted for publication: February 8, 1986)

Summary A new description of evoked potential activity in terms of 'dipole source potentials' is presented, based on the physical laws relating intracranial electrical activity and scalp potentials. Recorded at a sufficiently distant electrode, the electrical activity of a spatially restricted region can be approximated uniquely by a time varying dipole vector field with stationary equivalent dipole location. Each of its 3 projections on a 3-dimensional coordinate system presents an accordingly defined 'dipole source component.' Magnitudes of these components are functions of time, named 'dipole source potentials.'

The 2-dimensional coronal scalp distribution of middle and late AEPs, obtained in 15 normal subjects, could best be decomposed into tangential and radial dipole source components, originating from the auditory structures in both temporal lobes. Initial tangential activity (N19t-P30t) appeared to arise in primary auditory cortex, and initial radial activity (N27r-P39r) in secondary auditory cortex, in view of the similarity with intracranial records (Celesia 1976). Unilateral lesions of the acoustic radiation abolished ipsilateral MAEP dipole source potentials. Lesions involving AI/II and AAI also abolished the LAEP source potentials in the damaged hemisphere. The normal dipole source potentials in the intact hemisphere fully explained scalp distributions in these patients. In cases with assumed interruption of primary cortical input, presence of late dipole source potentials, which were delayed by 20–30 msec, probably reflected cortical activation via commissural fibres.

Keywords: *auditory evoked potentials (AEPs) – dipole source potentials – spatio-temporal dipole model – auditory cortex – temporal lobe lesions*

The value of evoked potentials (EPs) in the assessment of neurological disorders could be considerably enhanced if EP components were unambiguously relatable to the neuroanatomical substrate. In principle, this requires a decomposition of scalp potentials into 'source potentials,' such that each source potential reflects the compound local activity of a circumscribed brain region. Yet conventionally, EP components are defined by the sequence or latencies of prominent peaks or by characteristics in scalp distribution. Thus, the major deflection in the auditory evoked potential (AEP), first described by Davis (1939), is synonymously known as N1-P2, N100-P180 or 'vertex potential.' Numerous other peaks have been described for the middle (MAEP) and late (LAEP) latency components of the AEP (Picton et al. 1974; Wolpaw and Penry 1975; Goff et al. 1977; McCallum and Curry 1979; Wood and Wolpaw 1982; Polich and Starr 1983; Perrault and Picton 1984). A general description of all AEP components in terms of source activity has not yet been given.

In man, definition of components in the sense of 'source potentials' depends primarily on complementary evidence obtained by scalp distribution studies of electrical and magnetic fields and analysis of equivalent dipole sources, by alterations due to circumscribed lesions, by comparison with intracranial recordings and from appropriate animal models (Vaughan 1982; Wood et al. 1984). The scalp distribution of middle and late AEPs, which is symmetrical around and maximal over the vertex, has been analysed in detail (Vaughan and Ritter 1970; Picton et al. 1974; Cohen 1982; Wood and Wolpaw 1982), but interpretations of polarity reversal and influence of the reference electrode remain controversial (Kooi et al. 1971; Wolpaw and Wood 1982). Recently, an almost identical approximation of the LAEP

[1] Address for correspondence: Dr. Michael Scherg, Max Planck Institute for Psychiatry, Dept. of Neuropsychology, Kraepelinstr. 10, D-8000 Munich 40, F.R.G., Phone: 089/30622-260.

coronal scalp distribution by the overlapping activities of two bilateral dipole sources in the temporal lobes has been demonstrated (Scherg and Von Cramon 1985a), in accordance with neuromagnetic source locations (Hari et al. 1980). Preliminary results from a spatio-temporal dipole model of the MAEP scalp distribution indicated comparable dipole locations for the major middle latency component Na-Pa (N19-P30) (Scherg 1984a).

In patients with unilateral temporal lobe lesions hemispheric asymmetries of the LAEP (Peronnet et al. 1974; Knight et al. 1980; Michel et Peronnet 1982) and of the MAEP (Gerull et al. 1981; Kraus et al. 1982) have been described. Findings in patients with bilateral temporal lobe lesions range from complete abolition of middle (Özdamar et al. 1982) and late (Jerger et al. 1969; Michel et al. 1980) potentials to reportedly normal AEPs (Parving et al. 1980; Woods et al. 1984). These conflicting results raise questions on the extent of the temporal lobe structures generating the AEP.

This study introduces the concept of 'dipole source potentials' and gives a concise definition of MAEP and LAEP activity in terms of tangential and radial 'dipole source components.' Selective abolition of 'dipole source potentials' in cases with unilateral vascular lesions is demonstrated.

Methods

Subjects and recording conditions

AEPs were obtained from a group of 10 female and 5 male normal subjects between the ages of 21 and 46 with no history of neurological or audiological problems. Subjects had pure tone audiometric thresholds up to 20 dB at 1000 Hz and 30 dB at 4000 Hz. AEPs were also recorded in 28 patients (18 males, 10 females, age range 36–74) with circumscribed vascular brain lesions, who were submitted for central hearing diagnosis from the neuropsychological department of the city hospital in Bogenhausen. Auditory cortical areas which were presumably affected, according to CT scan evaluation, were classified as AI/AII, AAI and AAII (Pandya and Seltzer 1982). In this study only CT and AEP data of this patient group are presented, along with a more detailed description of 3 typical cases. Audiological test results will be reported elsewhere (Scherg and Von Cramon 1986).

Subjects were seated comfortably in a reclining position in a sound-treated and electrically shielded room. Stimuli were monaural, alternating, 70 dB HL clicks (0.1 msec duration) and tone bursts (1000 Hz, 20 msec on/off with a cosine (cos**4) shaped envelope, no plateau) for MAEP and LAEP recordings, respectively, with a pseudo-random interstimulus interval of 95–135 msec and 1.5–2.5 sec respectively. Virtual trigger time (Brinkmann and Scherg 1979) of tones was defined at 6 msec.

An 11-channel recording montage along a tilted coronal plane was used with a vertex electrode (3 cm in front of Cz), a neck electrode over C5 (assigned to 140° in the y–z plane of the head model) and 5 electrodes over each hemisphere which were equidistantly spaced from the vertex electrode to each mastoid (lowest electrode approximately 4 cm behind and 1 cm below tragus; ±120° in x–z plane). The vertex electrode was used as recording reference to allow inspection of waves V, N19-P30 and N100 during averaging as usual. Recording parameters for MAEP (LAEP) were sweep lengths of 60 (400) msec with 5 (0) msec prestimulus baselines, digitization intervals of 0.12 (1) msec, a common time constant of 1 sec and antialiasing filters (Bessel, 24 dB/octave) of 2000 (200) Hz. Before analysis, signals were digitally filtered (Scherg 1982a) with a zero-phase-shift bandpass of 20–300 (3–50) Hz to minimize low frequency noise and to permit decimation to 50 digitization points/trace. For display and analysis signals were rereferenced to the average reference (Scherg and Von Cramon 1984).

Two thousand (64) sweeps were averaged in a run. Five averages were, alternatingly, obtained per ear (3 MAEP runs/ear in patients to restrict recording time to 50 min). Sessions began with LAEP recordings and subjects were instructed to listen to the stimuli without counting and to keep their eyes open. For the subsequent MAEP recordings, light was dimmed and subjects allowed to fall asleep. Simultaneously recorded BAEPs (Scherg 1982b) monitored adequate auditory input

at the brain-stem level, controlled by wave V latency.

Derivation of dipole source potentials

The spatio-temporal dipole model (STDM), presented in detail previously (Scherg 1984b; Scherg and Von Cramon 1985a,b), was used to determine locations, orientations and temporal course of activity of equivalent dipole sources. It was realized that the restriction to model dipole wave forms of triphasic shape often required 3 or 4 sources in each temporal lobe for a full description of scalp AEPs (Fig. 1A). This entailed cumbersome calculations with non-unique, yet mathematically equivalent, solutions of the fit procedure. Also, practical clinical use of STDM in this form seemed impossible. Two reasons for this problem were found:

(1) Small changes in AEP dipole locations (10% of the head model radius R) induced variations in simulated scalp potentials which were well below the usual noise level in measured signals.

(2) Model wave forms depended on equivalent dipole orientations. Hence, more or different constraints, either spatial or temporal ones, were required for a unique definition of dipole source components.

For the first reason, the electrical activity of a restricted intracranial region of 2–2.5 cm in diameter may be well approximated by a dipole source located at the centre of this region ($\vec{r}$) having a dipole moment vector $\vec{m}(t)$

$$\vec{m}_i(t) = \left(m_{xi}(t), m_{yi}(t), m_{zi}(t)\right) \qquad (1)$$

which is separable into its 3 projections on a defined coordinate system (Fig. 1). Each projection represents a dipole with constant location $\vec{r}$ and orientation $\vec{o}_j$ (j = x, y, z) and with time varying strength $m_j(t)$. A dipole projection thus obtained is named 'dipole source component' and its magnitude $m_j(t)$, scaled in voltage units comparable to surface voltage, is named a 'dipole source potential.'

The scalp potential u at electrode k is determined by superposition of the 3-D (2-D) dipole source potentials contributed by NS (number of sources) hypothesized regional sources:

$$u_k(t) = \sum_{i=1}^{NS} \vec{m}_i(t) \cdot \vec{d}(\vec{r}_i, \vec{e}_k) \qquad (2)$$

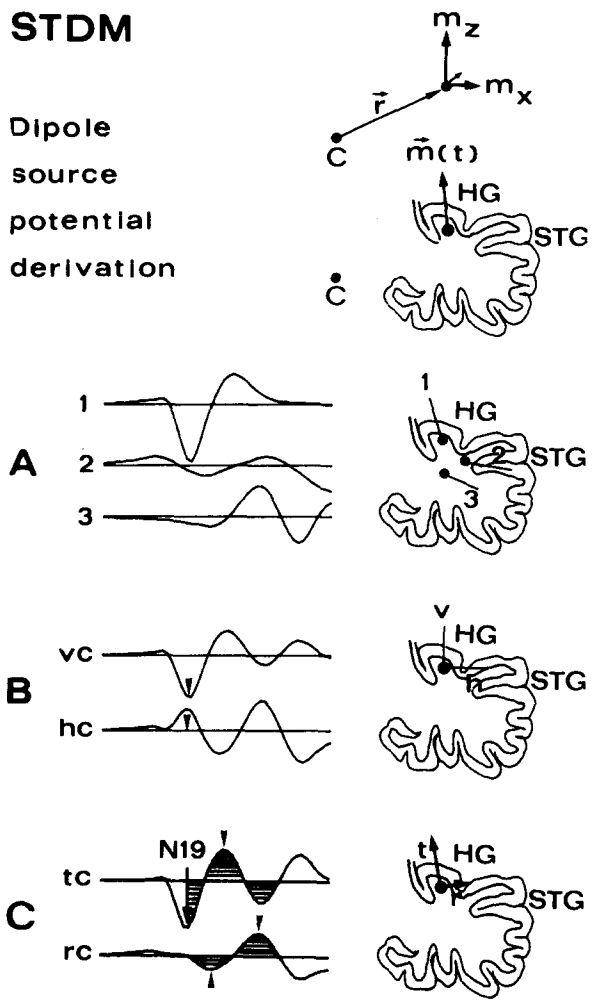

Fig. 1. Spatio-temporal dipole model (STDM) and dipole source potential derivation. A dipole source is defined by the stationary location $\vec{r}$ relative to the centre c of the head model, and by a time varying dipole moment vector $\vec{m}(t)$, with coordinates m_x and m_z in the coronal plane (top). $\vec{m}(t)$ is depicted in a schematic frontal section of the right temporal lobe (HG = Heschl's gyri, STG = superior temporal gyrus), with location and orientation as obtained at t = 19 msec (peak of primary activity) for a normal subject (same as in Fig. 2). Right hemispheric MAEP activity can be completely described by 3 STDM sources with (filtered) triphasic wave forms (A), or almost identically by the vertical (vc) and horizontal components (hc) of a regional equivalent source (B) having multiphasic wave forms. Finally, the projection coordinate system is rotated to maximize primary (N19) activity (C). Components thus obtained are practically tangential (tc) and radial (rc). Their wave forms are 'dipole source potentials' by definition. Shaded area indicates interval over which effective dipole moment (invariant under rotation!) is computed.

with the 3-D vector $\vec{d}$ containing dipole model dependent geometrical weighting coefficients, reflecting the contribution of a unit dipole moment vector located at $\vec{r}$ to an electrode located at $\vec{e}_k$. For each instant t, eqn. 2 forms a set of NE (= no. of electrodes) linear equations, allowing the calculation of NC instantaneous dipole source voltages m by linear optimization, if NC is less than NE and if the NE − 1 recording channels are linearly independent. For the present AEP data unit dipole source potential was scaled to unit voltage in a C3-A1 for a tangential dipole located in the coronal plane at $r = 0.59$ R (theta = 70°, spherical 3-shell head model, Scherg and Von Cramon 1985a).

Only two regional sources, one for each temporal lobe were assumed to model both the MAEP and LAEP coronal scalp distributions. In order to obtain a unique description of components, for each source a specific projection coordinate system had to be selected, because rotation of this coordinate system produces a set of linearly transformed wave forms while the underlying 3-D dipole field is invariant. Selection of a particular coordinate system can therefore be based on morphological constraints, without changing the accuracy of the approximation. Therefore, from the MAEP recordings in the 2-D coronal plane dipole source components were determined first along the vertical and horizontal axes (Fig. 1B). Then the rotation angle was calculated which maximized the N19 peak, thus obtaining the orientation of the primary temporal lobe activity. Because the resulting orientation closely corresponded to a tangential projection (Fig. 1C), the major peaks of this dipole source component were labelled N19t, P30t and peaks of the orthogonal (radial) component were labelled N27r and P39r, to distinguish the various scalp-recorded peaks.

To test clinical applicability, 3 approaches for the derivation of dipole source potentials have been investigated in parallel:

(a) Best fit STDM solutions were obtained for neural activity from both temporal lobes and, in MAEP analysis only, also for myogenic activity and brain-stem slow wave V. Then, scalp potentials were replaced by model activity due only to the temporal lobe sources, thus free from myogenic contamination. Dipole source potentials were calculated for the 4 tangential and radial components in both hemispheres by solving eqn. 2. Difference in variance between this and STDM solutions was usually less than 1% of total variance. Signals were smoothed once before and after solving eqn. 2 by a 3-point weighted average (0.25, 0.5, 0.25).

(b) Dipole source potentials were calculated directly from the 12 electrode voltages, solving eqn. 2. Electrodes apparently containing myogenic or (in 2 cases) artefactual activity were excluded prior to analysis (mostly 1 or 2 mastoid electrodes). Smoothing as in (a).

(c) For each hemisphere two bipolar derivations were computed from the first electrode relative to the third (channels 2/4) and fourth (channels 1/3) lateral electrodes, counting from the vertex electrode. This appeared to be the best selection out of the 12 electrodes used, with no more than an acceptable amount of myogenic contamination. From this 4-channel montage 4 dipole source potentials could be computed by linear combinations, assuming symmetrical inward inclination of 17° for the tangential dipoles. Weight coefficients were 1.114, −0.650, −0.374, 0.303 (channels 1–4) for right hemisphere tangential and 0.948, −1.650, 0.185, −0.201 for radial dipole source potentials. Channels 1/2 and 3/4 exchange for left hemispheric dipole source potentials. Smoothing as in (a).

Quantitative evaluation of dipole source potentials

For each condition (hemisphere; side of stimulation) the root mean square magnitude of the dipole moment vector m (DMrms), i.e., the mean effective dipole strength over a defined time interval (19–45 msec for MAEP, 45–200 msec for LAEP) was determined, this parameter being invariant to rotations of the projection coordinate system. DMrms was scaled to equate mean normal (across conditions and subjects) tangential amplitudes, defined below. Lengths of dipole vectors, as depicted in the figures, were defined by relative areas underlying dipole source potentials in these intervals (Fig. 1). Maxima and minima of every dipole source potential were evaluated by an automatic 1st derivative zero-crossing algorithm.

Latencies of the main MAEP peaks N19t, P30t, N27r and P39r were treated as missing values if they exceeded a range of 15–26, 24–38, 21–35, 30–48 msec respectively. Allowable ranges for LAEP peaks were: 45–200 msec (N100t), 120–240 msec (P180t), 75–135 msec (P100r) and 110–200 msec (N150r). Amplitudes were defined by peak-to-peak measures of maximal transients in dipole source potentials. Right (RH) and left (LH) hemispheres were compared by computing mean parametric values averaged over values obtained for right and left ear stimulation and their difference (RH-LH). Confidence intervals in hemispheric differences were defined by 3 standard deviations (S.D.s). Hemispheric differences were preferable to ratios (Wolpaw and Penry 1977) because they were less affected by residual noise in cases having small amplitudes, while 3 S.D. limits were comparable. For all parameters, right versus left ear and ipsi- versus contralateral pathway differences were also obtained and significances assessed (paired t test).

Results

MAEP dipole source potentials in normal subjects

The MAEP coronal scalp distribution of a normal subject and the best fit STDM wave forms (unexplained variance only 3%) are plotted in Fig.

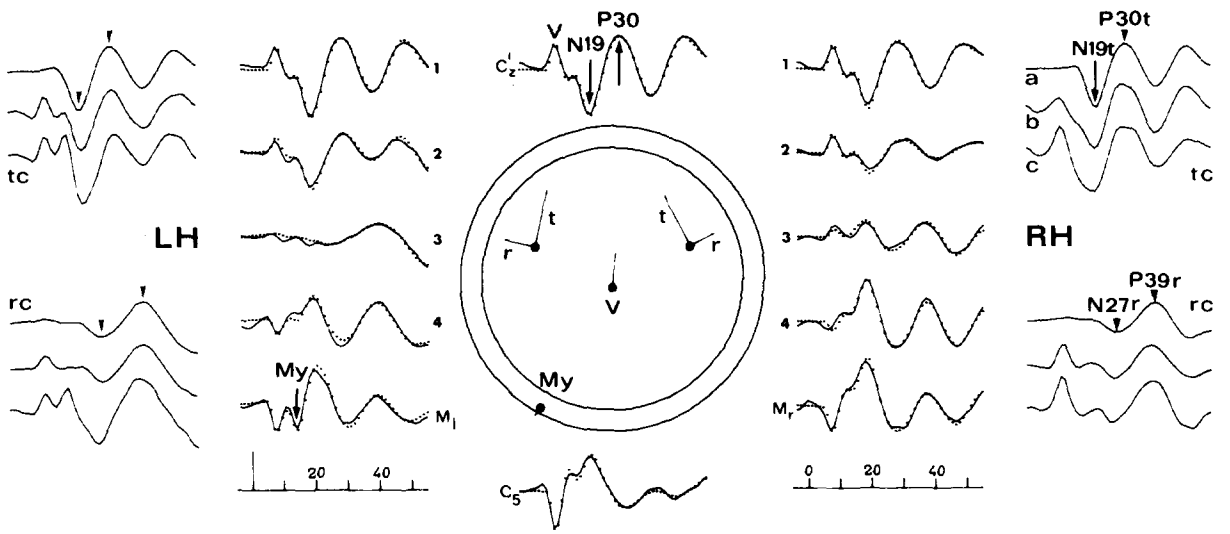

Fig. 2. MAEP coronal scalp distribution of a normal subject, right ear click stimulation, average of 10,000 sweeps. Around the schematic frontal section of the head model (outer circle: scalp, inner circle: dura) MAEP wave forms (solid lines) are depicted as recorded from the vertex (Cz′ = 3 cm in front of Cz, top trace), from the neck (C5, bottom) and from the right (RH) and left (LH) hemispheres. The lateral electrodes (1–4) were equally spaced between Cz′ and the mastoids (M_r, M_l). Average reference computed over these 12 electrodes, time scale in msec, vertical mark on left at time of click delivery (0 msec) equals 500 nV. Superimposed dotted traces are best fit signals obtained by the spatio-temporal dipole model. Dipole inserts show location (dot), orientation and relative strength (line) of tangential (t) and radial (r) dipole source components in both temporal lobes and of wave V (V) and myogenic (My) components. In the corners on both sides dipole source potentials are shown for the temporal lobe tangential (tc, upper half) and radial components (rc, lower half). Each set of 3 dipole source potentials presents solutions obtained by approaches a (top trace), b (middle) and c (bottom) for comparison. Peaks in the dipole source potentials are labelled by a polarity-latency-orientation nomenclature (N/Pxxxt/r). Main transients of the tangential (N19t-P30t) and radial (N27r-P39r) dipole source potentials are indicated by arrows in both hemispheres for solution a. Note the larger contamination by myogenic and wave V activity in the solution c, obtained from the 4-channel montage which comprised only electrodes 1, 3 and 4. Note also that the use of the average reference leads to an apparent polarity reversal of tangential activity near the sylvian fissure and partly unravels the laterally oriented activity at electrodes 3.

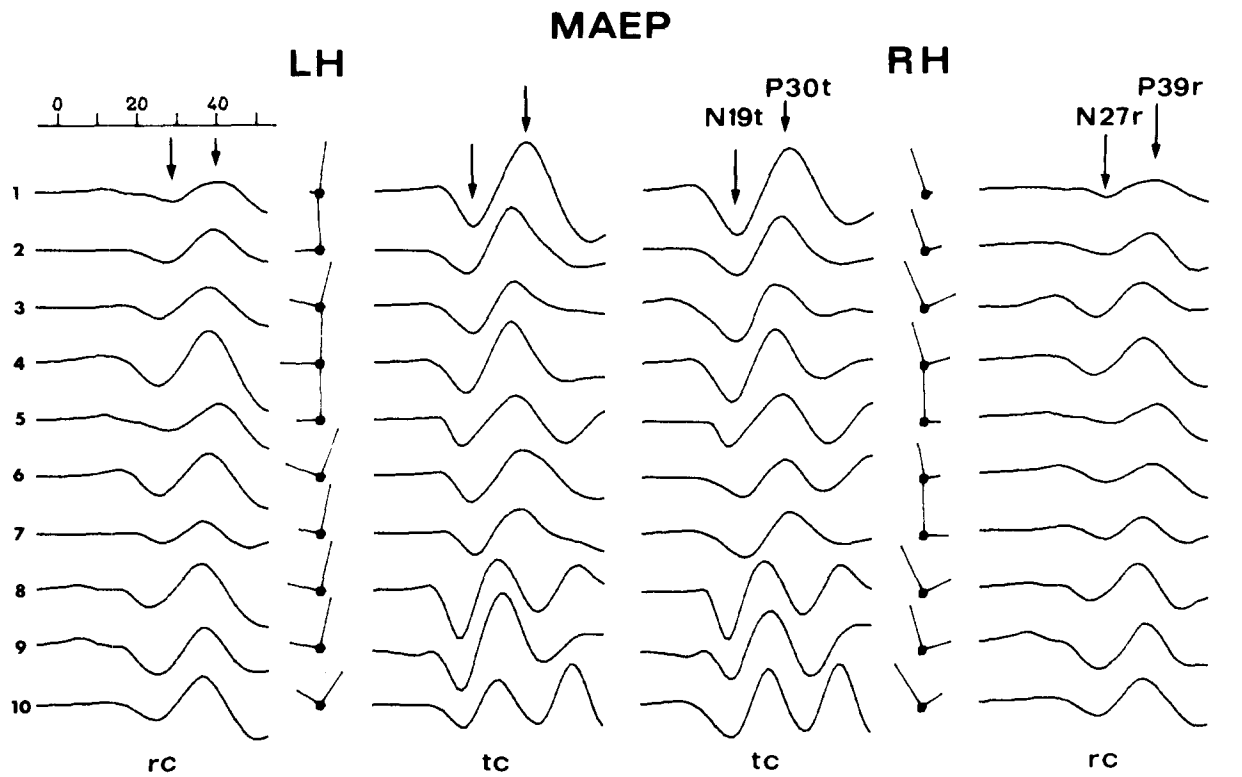

Fig. 3. MAEP dipole source potentials obtained in 10 normal subjects (1–10). Scales as in Fig. 2. Wave forms of tangential (middle traces) and radial components (lateral traces) are comparable in right (RH) and left (LH) hemispheres, while amplitudes are in most cases slightly larger contralateral to the stimulated (right) ear. Dipole inserts (as in Fig. 2) illustrate the small variability in orientation of primary N19t. Note the similarity in wave form of N27r-P39r across subjects and the greater variability of tangential activity after N19t.

2. Potential traces at the vertex show the typical pattern of slow BAEP wave V followed by the prominent N19-P30 complex and a second negative-positive wave (Nb-Pb) which was seen only in a minority of subjects. Wave form changes were remarkable at the lateral electrodes and an inverted pattern was observed at lower electrode sites with a myogenic component superimposed at the left mastoid electrode. Dipole source potentials were very similar in the two hemispheres, with tangential peaks N19t-P30t resembling the scalp potential at the vertex and radial peaks N27r-P39r not as clearly emanating at scalp sites due to the complex spatio-temporal overlap of source activities. The normal MAEP dipole source potentials exhibited great similarity in wave form between subjects (Fig. 3). Also, orientation of the earliest activity from the temporal lobes (N19t) was approximately tangential for all subjects (Fig. 3) with an S.D. of only 7° for right and 11 for left hemispheric dipoles (Table I). When dipole location, symmetrical in the two hemispheres, was allowed to vary in order to find the best fit to the

TABLE I

Dipole source parameters.

	Location		Orientation ($N19_{max}$, $N100_{max}$)		
	Eccentricity (unit radius)	Theta (degrees)	RH	alpha (degrees)	LH
MAEP	0.55 ± 0.07	68 ± 10 (11)	−20 ± 7		14 ± 11 (15)
LAEP	0.60 ± 0.08	81 ± 9 (12)	−43 ± 14		38 ± 12 (15)

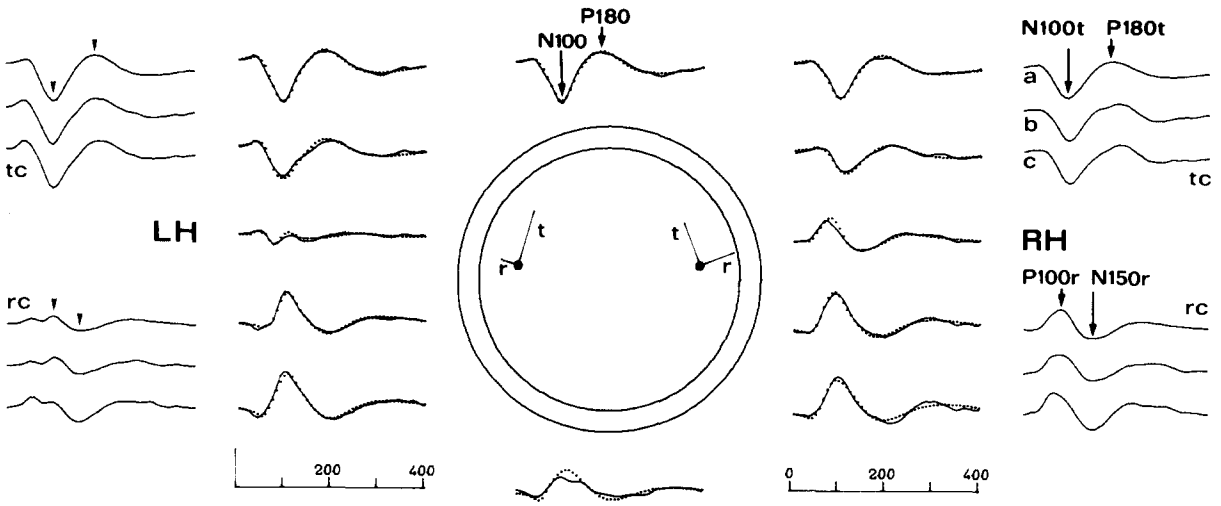

Fig. 4. LAEP coronal scalp distribution, right ear stimulation, 1000 Hz tone burst, 320 averages. Same subject and illustration as in Fig. 2, except for longer time scale (msec) and 10-fold amplitude (vertical mark = 5 μV). Main tangential (N100t-P180t) and radial transients (P100r-N150r) of the LAEP dipole source potentials are marked by arrows. Note the similarity of solutions a–c, which is mainly due to the lack of myogenic overlap at these latencies.

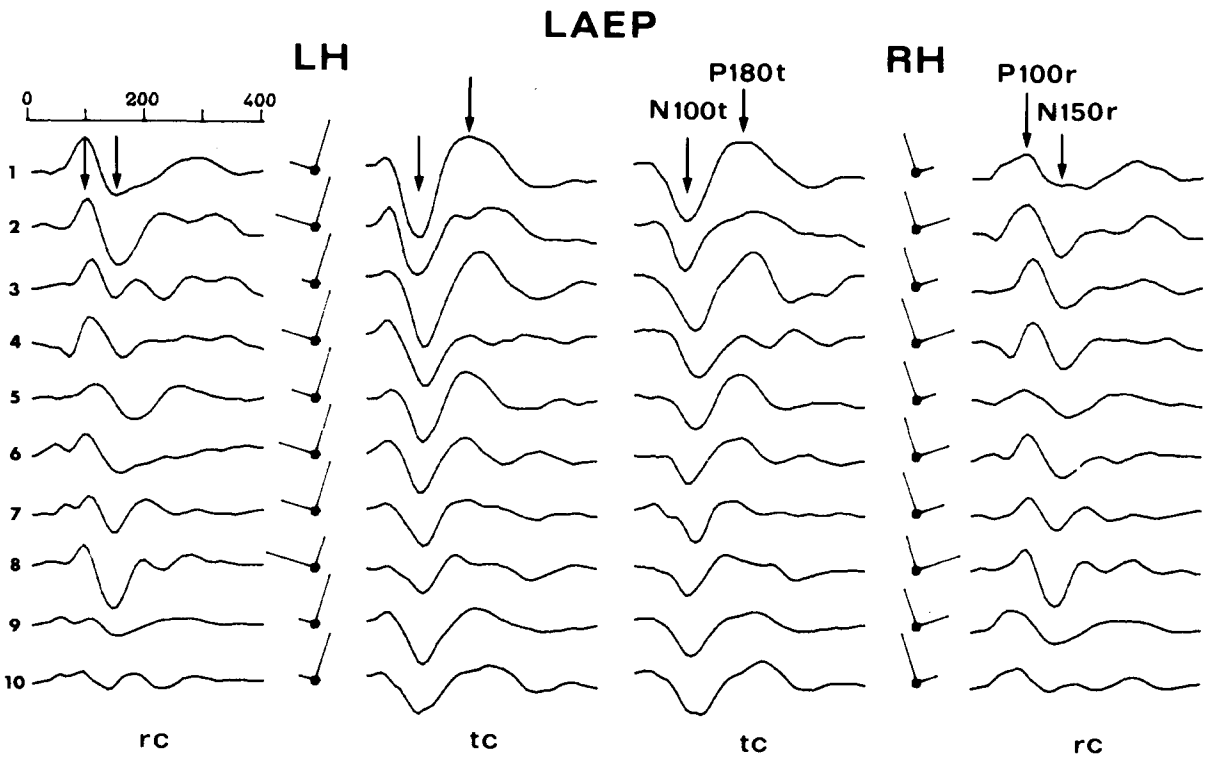

Fig. 5. LAEP dipole source potentials obtained in 10 normal subjects using fixed tangential and radial axes along the mean MAEP orientations. Scales as in Fig. 4, right ear stimulation. Note the similarity of N100t across subjects and the variability of radial wave forms and of P180t (in latency).

measured scalp distribution (approach b), in 11 subjects convergence of fit was obtained with a mean location of 55% of the head radius and an S.D. of only 7%.

LAEP dipole source potentials in normal subjects

Similar, although somewhat lower and slightly more eccentric, locations were found for the temporal lobe equivalent dipoles, best fitting the LAEP scalp distribution in 12 subjects. When the activity at 100 msec was maximized similarly to N19, the equivalent dipoles were tilted inwards by almost 45°, indicating overlap of tangential and radial activities (Table I). Because the tangential mean orientation of the N19 activity seemed to reflect the effective electrical field projection of primary auditory cortex (AI), LAEP dipole source potentials were calculated, using mean normal MAEP orientations. Thus, it was found that the normal LAEP scalp distribution (Fig. 4) could be well described by a tangential activity (N100t-P180t) resembling the 'vertex potential' and a radial activity with more variable wave form (P100r-N150r). The previously described P210 peak (Scherg and Von Cramon 1985a) was not as prominent under the present stimulus and recording conditions (Fig. 5). In some subjects P100r peaked clearly before N100t. Model wave forms at the neck electrode conformed less with LAEP as compared to MAEP signals, possibly indicating the influence of source activity perpendicular to the coronal plane or inaccuracy of the spherical head model for lower electrode sites.

Dipole source potential parameters

Mean values of effective dipole moment (DMrms), amplitudes of prominent transients and latencies of dipole source potentials in both hemispheres are given in Table II. For each subject, values of right and left ear stimulation were averaged. MAEP mean values obtained by approaches a and b were very similar, with practically identical confidence limits. Variation in latency, particularly of peaks N27r, P39r, N100t, P100r and N150r was surprisingly small. In the control group, hemispheric differences in amplitudes and latencies

TABLE II

Dipole moment, amplitude and latency of dipole source potentials.

Parameter	Unit	RH	LH	RH-LH	Limit
Dipole moment					
MAEP	μV_{eff}	0.62 (0.15)	0.61 (0.16)	0.01 (0.074)	40/50%
LAEP	μV_{eff}	5.4 (1.7)	5.6 (1.9)	0.14 (0.616)	35/60%
Amplitude					
N19t-P30t	μV	0.62 (0.16)	0.61 (0.18)	0.01 (0.09)	50/55%
N27r-P39r	μV	0.31 (0.11)	0.32 (0.10)	−0.01 (0.06)	65/–%
N100t-P180t	μV	5.4 (1.9)	5.6 (1.9)	−0.25 (0.80)	50/–%
P100r-N150r	μV	3.8 (1.6)	3.7 (2.1)	0.02 (1.1)	–/–%
Latency					
N19t	msec	19.4 (1.1)	19.5 (1.3)	−0.18 (0.63)	3.5 msec *
P30t	msec	30.9 (2.0)	31.6 (2.0)	−0.61 (0.92)	4.5 msec *
N27r	msec	27.0 (1.4)	27.3 (1.4)	−0.31 (1.5)	4.9 msec *
P39r	msec	39.1 (1.4)	39.7 (1.6)	−0.71 (1.2)	5.0 msec *
N100t	msec	100 (6)	101 (5)	−0.3 (6.0)	18 msec
P180t	msec	195 (24)	185 (17)	11.0 (25.0)	–
P100r	msec	96 (6)	100 (5)	−3.7 (5.3)	−20 (+13)
N150r	msec	152 (7)	151 (7)	1.8 (4.3)	15 msec

Means (S.D.s). RH = right, LH = left hemisphere, RH-LH = hemispheric difference, limit = 3 S.D. confidence limit for 12-channel/4-channel evaluation.

* Measurement error of 1 msec has been added.

(right and left ear averages) were either not significant or only weakly ($P < 0.05$) significant for P30r, P39r and P100r, peaking earlier in the left hemisphere (Table II). Because of the small interhemispheric variability, abnormalities in one hemisphere could be detected (3 S.D. limit) if DMrms was reduced by only 40% of the normal magnitude. Using the 4-channel approach c, the 3 S.D. limit was 50% (60), a value which was exceeded in many patients. Highly significant pathway differences were found for the LAEP with greater dipole moment (by 11%) amplitudes and earlier latencies contralaterally (Table III). Contralateral dipole moment and amplitudes of the MAEP differed less from ipsilateral values. In contrast to tangential components, the radial MAEP component appeared earlier on the ipsilateral site.

TABLE III

Contralateral versus ipsilateral differences.

Parameter	Unit	CL-IL	Sig
Dipole moment			
MAEP	μV_{eff}	0.04 (0.066)	*
LAEP	μV_{eff}	0.69 (0.358)	***
Amplitude			
N19t-P30t	μV	0.03 (0.07)	NS
N27r-P39r	μV	0.06 (0.07)	**
N100t-P180t	μV	0.70 (0.37)	***
P100r-N150r	μV	0.19 (0.45)	NS
Latency			
N19t	msec	−0.43 (0.58)	*
P30t	msec	−0.22 (1.0)	NS
N27r	msec	0.77 (1.2)	*
P39r	msec	0.74 (1.0)	*
N100t	msec	−4.8 (3.4)	***
P180t	msec	−5.0 (24.0)	NS
P100r	msec	−3.1 (1.8)	***
N150r	msec	−2.5 (4.2)	NS

CL = contralateral, IL = ipsilateral.
Significances: * $P < 0.05$, ** $P < 0.01$, *** $P < 0.001$.

Dipole source potentials in patients

In patients two distinct types of AEP abnormality were observed. Type I was a significant unilateral reduction of both MAEP and LAEP dipole source potentials. This was observed in 14 patients with unilateral lesions, most probably involving the auditory cortex (AI/AII, AAI) and the distal portion of the acoustic radiation, according to CT scan evaluation (Table IV). Type II abnormality consisted in a unilateral reduction of MAEP dipole source potentials with preserved but, in most cases, delayed LAEP dipole source potentials in the damaged hemisphere. This pattern was seen in 9 patients with lesions probably involving only the acoustic radiation and sparing the auditory cortex. In 4 of these cases the CT scan did not give unambiguous evidence of involvement of the acoustic radiation while the reduction of MAEP source potentials on the side of the infarction was highly significant. Reduction was mostly down to noise level, indicating complete unilateral abolition of source activity (cf., Figs. 6 and 7). In most cases amplitude asymmetry was observed on stimulation of either ear, although in general MAEP and LAEP amplitudes were slightly larger on stimulation of the ear contralateral to the intact hemisphere, reflecting contralateral pathway dominance. In a few cases with small amplitudes the mean hemispheric difference in dipole moment was within 3 S.D.s of the normal distribution, but exceeded 2.5 S.D.s (cases 12–16). In 5 patients, with lesions which most probably spared both auditory cortices and acoustic radiations, no hemispheric asymmetries were found (Table IV).

Case reports

MAEP and LAEP scalp distributions of two

Fig. 6. MAEP coronal scalp distribution and dipole source potentials of patient cases A–C, each illustrated as in Fig. 2. Note the apparent loss of tangential and radial activity in the damaged hemisphere in all cases (stimulation contralateral to intact hemisphere in cases A and B; for case C right and left ear MAEPs were averaged). Despite a higher noise level in the instantaneous solutions b and c, the alterations of the tangential and radial components on the damaged side are clearly evident. Dipole source potentials in the intact hemisphere are as in normals (similar temporal lobe location!) and fully explain the scalp distribution which is non-zero over the damaged side. Overlap of tangential and radial activity from the same (!) equivalent dipole source leads to dramatic shifts of latency towards lower electrodes (arrowheads, cases A and B). Myogenic activity is fully separated in the STDM solutions and contributes substantially only in the 4-channel approach in case C, due to myogenic overlap at lateral electrodes (arrowheads).

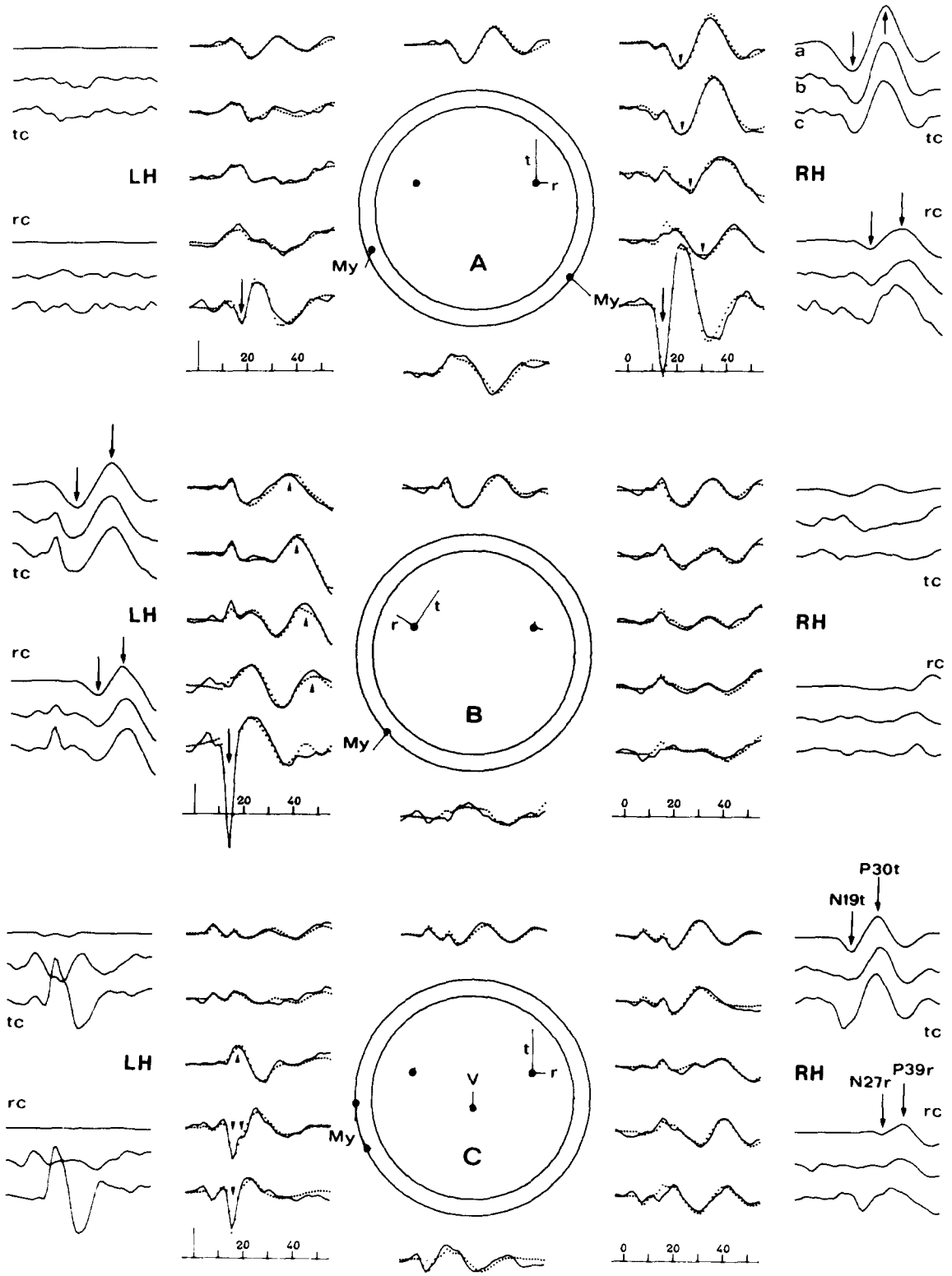
tc
LH
rc
20
40
My
A
t
r
My
0
20
40
a
b
c
tc
RH
rc
tc
LH
rc
20
40
r
t
B
My
0
20
40
tc
RH
rc
tc
LH
rc
20
40
t
r
V
My
C
0
20
40
P30t
N19t
tc
RH
N27r
P39r
rc

TABLE IV

Relation between lesion location and changes in source potentials.

Case no.	Age	Sex	Aetiology type	Lesion location from CT						DMrms reduced		Delay LAEP
				Hem	PAR	DAR	AI/II	AAI	AAII	MAEP	LAEP	
1	74	f	MCAI (AB)	L	–	–	–	–	–	N	N	N
2	70	m	MCAI (PB)	L	–	–	?	+	+	N	N	N
3	60	f	PCAI (MAB)	L	–	–	–	–	–	N	N	N
4	49	f	PCAI (MAB)	R	?	–	–	–	–	N	N	N
5	50	m	PCAI	R	?	–	–	–	–	N	N	N
6	63	m	MCAI (PB)	L	–	+	+	+	–	L **	L **	–
7	58	m	MCAI (PB)	L	–	+	+	+	?	L **	L **	–
8	69	m	MCAI (PB)	L	–	+	+	+	?	L **	L **	–
9	60	f	MCAI (PB)	L	–	+	+	+	+	L **	L **	–
10	48	f	MCAI (PB)	L	–	+	+	+	–	L **	L **	–
11	50	m	MCAI (ST)	L	–	+	+	+	+	L **	L **	–
12	49	f	MCAI (ST)	L	–	+	+	+	?	L **	L *	–
13	52	f	MCAI (ST)	L	–	+	+	+	+	L **	L *	–
14	64	f	MCAI (PB)	L	–	+	+	+	–	L *	L **	–
15	56	m	MCAI (PB + LSA)	L	–	?	+	+	?	L *	L **	–
16	42	m	MCAI (PB + LSA)	L	–	?	?	–	–	L *	L **	–
17	47	m	MCAI (ST) + ACHAI	L	?	+	+	+	+	L **	L **	–
18	48	m	MCAI (ST) + ACHAI	R	+	+	+	+	+	R **	R **	–
19	36	m	MCAI (ST)	R	–	+	+	+	+	R **	R **	–
20	48	m	MCAI (LSA)	L	?	+	–	–	–	L **	N	L tc
21	53	m	MCAI (LSA)	L	–	+	–	–	–	L **	N	L tc
22	47	m	MCAI (LSA)	L	–	+	?	–	–	L **	N	L rc
23	66	m	MCAI (PB)	L	–	–	–	?	–	L **	N	N
24	53	m	MCAI (ST) + ACHAI	L	–	?	?	–	+	L **	N	N
25	46	m	MCAI (LSA) + ACHAI	L	?	–	–	–	–	L **	N	N
26	60	m	ACHAI	L	+	–	–	–	–	L **	N	L tc
27	52	f	ACHAI	L	+	–	–	–	–	L **	N	L rc
28	69	f	PCAI (MAB)	R	?	–	–	–	–	R **	N	R rc

MCAI = middle cerebral artery infarction; PCAI = posterior cerebral artery infarction; ACHAI = anterior choroidal artery infarction; LSA = lateral striate artery; PB/AB = posterior/anterior branches; ST = sub-total; MAB = mesencephalic artery branches; Hem = hemisphere; PAR/DAR = proximal/distal acoustic radiation; AI/AII/AAI/AAII = auditory cortical areas; +/?/– = certain/questionable/no affection; L/R = left/right hemisphere; N = normal hemispheric difference (less 2.5 S.D.s); DMrms = effective dipole moment; **/* = reduction more than 3/2.5 S.D.s; tc/rc = delay of tangential (N100t)/radial (N150r) component more than 3 S.D.s.

Fig. 7. LAEP coronal scalp distribution of patient cases A–C. Illustration and scales as in Fig. 4. Stimulated sides as in Fig. 6. Late dipole source potentials are almost zero in the damaged hemisphere in cases A and B, having infarctions presumably extending over AI/II and AAI, whereas in case C a lesion of the acoustic radiation only leads to delay of N100t (N130t) in the affected hemisphere. Tangential dipole source potentials in intact temporal lobes are normal, whereas radial wave forms seem altered in cases A and C. Lacking overlap by myogenic activity, LAEP dipole source potentials are very similar for the different solutions a, b, c. Note that in case B, due to a strong radial component, the scalp distribution differs little between hemispheres at the upper electrodes and hemispheric differences would be small with a linked earlobe reference.

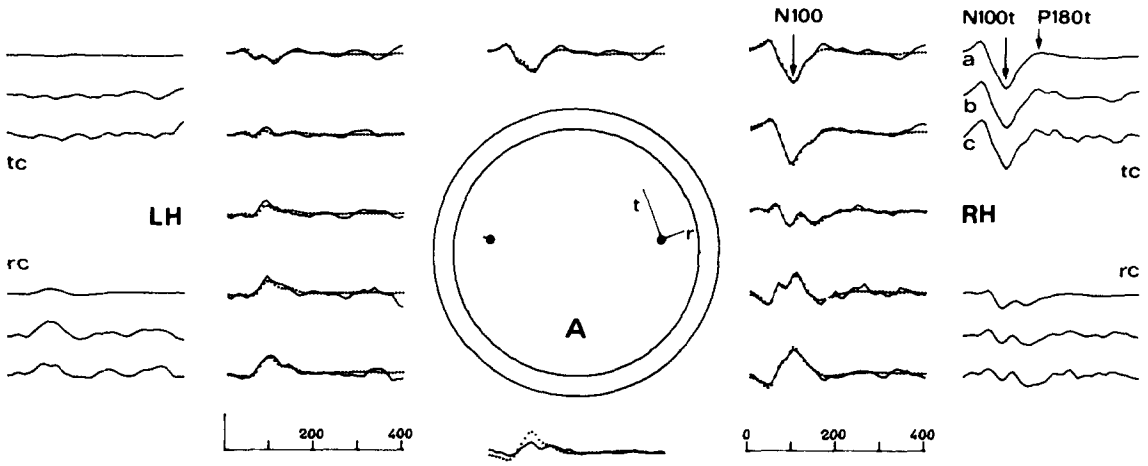
N100
N100t P180t
a
b
c
tc
LH
RH
rc
t
r
A
200
400
0

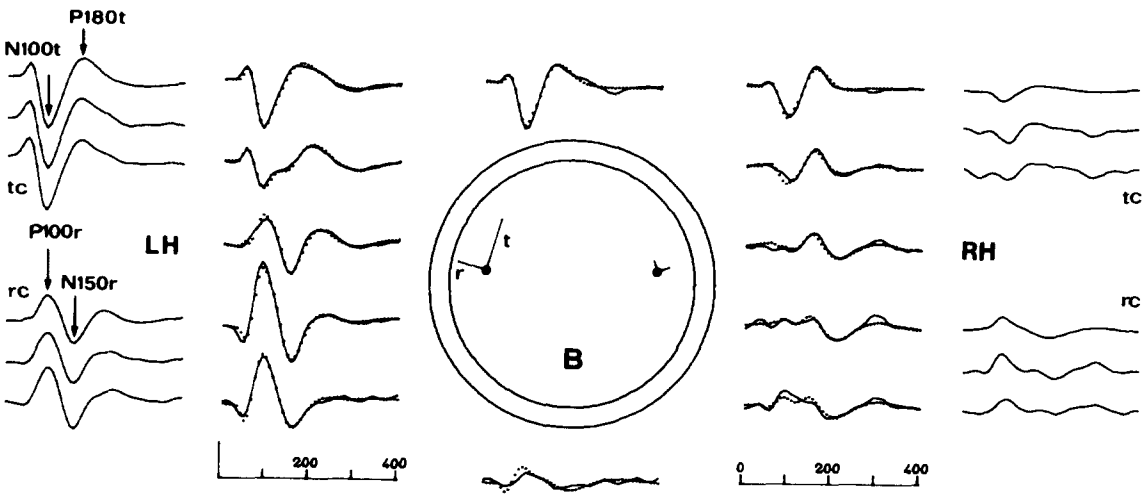
P180t
N100t
tc
P100r
N150r
LH
RH
rc
t
r
B
200
400
0

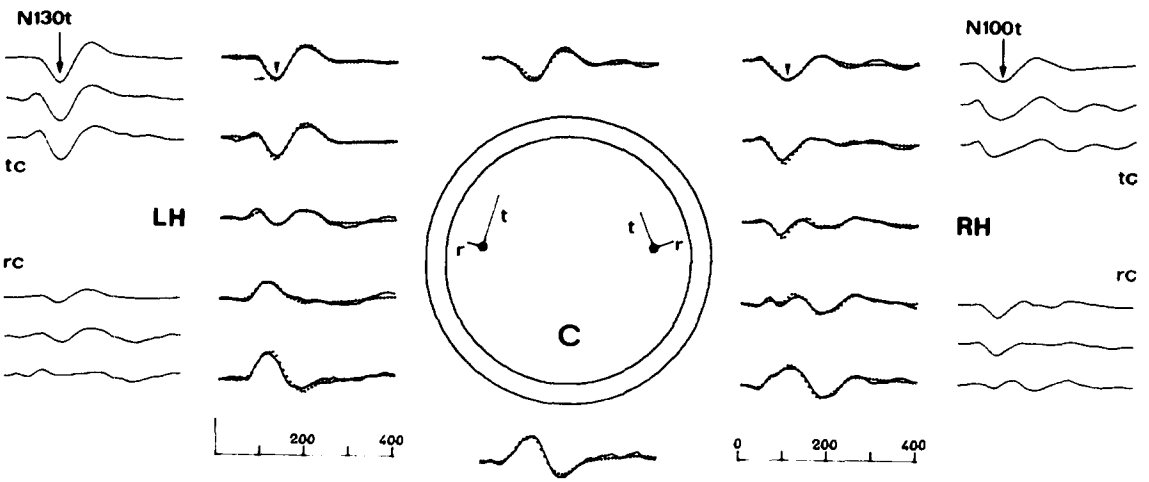
N130t
N100t
tc
LH
RH
rc
t
r
C
200
400
0

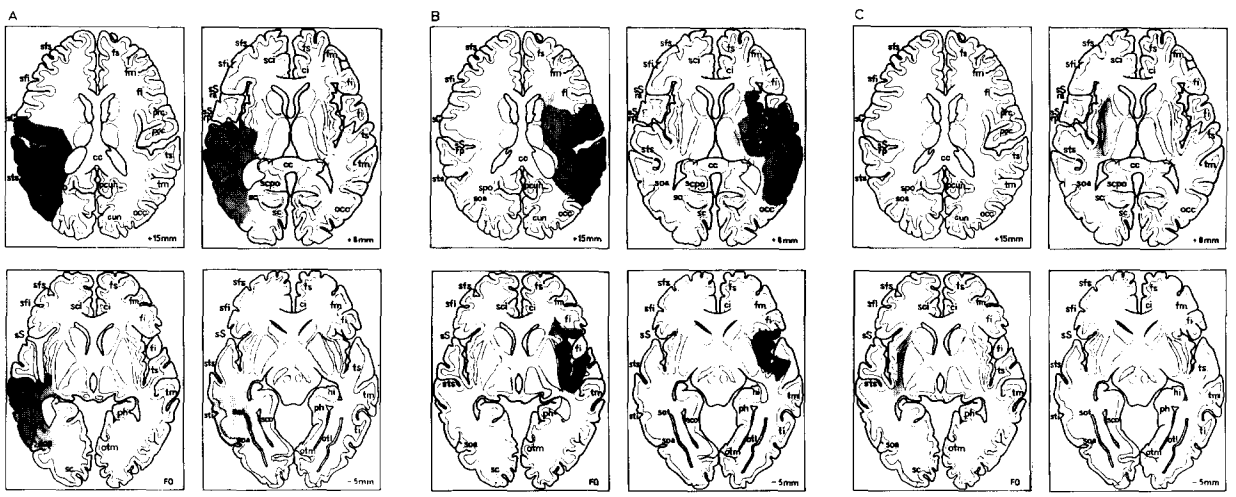

Fig. 8. Redrawings of horizontal CT scan sections of cases A–C at the level of the fronto-occipital (FO) line and at +15, +8 and −5 mm from FO level. In case A (left CT panel) the infarction apparently involved the distal portion of the acoustic radiation (DAR), Heschl's gyri (AI/AII) and a large part of the first auditory association area (AAI) on the left side. A certain amount of AAII may also have been affected. In case B (middle) the right hemispheric lesion presumably involved the proximal acoustic radiation (PAR) and DAR, AI/II, AAI (probably also AAII) as in case A. In case C (right) only the left acoustic radiation seemed to be covered by the lesion.

typical type I cases and of a type II case are shown in Figs. 6 and 7, along with dipole source potential solutions obtained by approaches a–c.

Case A (no. 8 in Table IV) was a 69-year-old male patient who had a Wernicke's aphasia after an ischaemic infarction of the posterior branches of the left middle cerebral artery, following a coronary bypass operation (description of lesion area in legend of Fig. 8A). He had normal pure tone thresholds. Testing was 6 months after the brain event. MAEP and LAEP scalp distributions were asymmetrical but signals were non-zero over the left hemisphere (Figs. 6 and 7). In contrast, the dipole source potentials of the left temporal lobe had practically vanished and the scalp distribution was fully explained by a regional source located in the right temporal lobe. Best fit locations using a unilateral source in this case and in cases B and C (MAEP only) coincided with the location of the bilateral sources in normal subjects, approximately corresponding to the position of Heschl's gyri. Myogenic activity in the MAEP was accounted for by superficial sources in the vicinity of both mastoids (Fig. 6).

Case B (no. 18) was a 48-year-old male patient suffering from a sub-total ischaemic infarction of the right middle cerebral artery and a partial infarction of the anterior choroidal artery, due to > 80% carotid siphon stenosis (cf., CT in Fig. 8B). He was tested 6 months after the incident and had a normal audiogram. AEP dipole source potentials showed an almost complete extinction of right temporal lobe activity. Again, the dipole source potentials in the intact hemisphere accounted for most of the observed scalp distributions. The MAEP scalp signals showed a conspicuous latency shift along left hemispheric electrodes, reflecting overlap of tangential and radial activities from the left temporal lobe (Fig. 6).

Case C (no. 20) was a 48-year-old male patient suffering from a left-sided ischaemic infarction in the territory of the lateral branches of the striolenticular arteries (cf., CT in Fig. 8C). Pure tone thresholds were elevated by 30–40 dB (500–4000 Hz) for the right ear and by 50–85 dB (500–4000 Hz; bone conduction thresholds 20 dB better) for the left ear. Testing took place 3 months after the brain event. With click levels of 80 dB (right) and 100 dB HL (left), BAEP wave V amplitude was symmetrical and latencies almost normal (5.7 msec for right, 6.0 msec for left ear stimulation). Hemispheric asymmetries obtained at these levels for

right and left ear MAEPs were comparable, indicating the relative independence of peripheral factors and the usefulness of simultaneous BAEP control. In Figs. 6 and 7 MAEP and LAEP scalp distributions, averaged over right and left ear stimulation, and dipole source potential solutions are shown for case C. Myogenic activity overlapping the MAEP over the left hemisphere was completely separated in the STDM solution, was greatly suppressed in the 12-electrode analysis by excluding the lower 3 electrodes but affected considerably the dipole source potentials obtained from the 4-channel montage (Fig. 6). Despite this myogenic overlap, an abolition of the typical MAEP pattern in the left temporal lobe was evident. In contrast, the LAEP dipole source potentials in this hemisphere showed no reduction, but a delay of 30 msec.

Dipole source potentials obtained by approaches a–c (Figs. 6 and 7) showed highly comparable wave forms apart from larger contaminations by noise and myogenic activity (only for MAEPs) in the direct instantaneous approaches b and c. Only in cases with large myogenic scalp activity was the 4-channel approach c more liable to project non-source activity onto dipole source potentials.

Discussion

The present results provide strong support for the generation of middle and late AEP activity in auditory cortical structures (AI, AII, AAI, Pandya and Seltzer 1982) for the following reasons:

(1) Best fit equivalent dipoles were located in or near to AI equally well for normal subjects and patients (in the undamaged hemisphere). These equivalent electrical dipole locations conformed with magnetic dipole locations derived from transient (Farrell et al. 1980) and steady state (Romani et al. 1982) middle latency and from transient late latency (Hari et al. 1980) auditory evoked fields (AEFs).

(2) Selective unilateral lesions of the acoustic radiation, probably depending on complete interruption of the primary afferent input to the auditory cortex, abolished the MAEP dipole source potentials. Late activity on the damaged side was undiminished but delayed by 20–30 msec in most cases. This probably reflected indirect activation of the preserved auditory cortex by commissural pathways from the undamaged hemisphere.

(3) Lesions fully comprising AI, AII and AAI also abolished the late, auditory evoked, dipole source potentials.

(4) Peaks and wave forms of derived tangential MAEP dipole source potentials were highly similar to potentials recorded from the superior temporal plane in man (N1-P2, 19–32 msec: Celesia 1976). Radial dipole source potentials conformed with records from the perisylvian area (N0-P1, 24–40 msec; P2-N2, 98–142 msec: Celesia 1976; P90-100: McCallum 1980). Although considerably larger in scalp records than primary MAEP components (by a factor of 6–8), the N100t-P180t component did not as clearly appear in intracranial records, possibly because of a more extended origin in the superior temporal plane (3-fold increase in diameter of active area entails a 9-fold decrease in local potential!).

(5) Considering differences in head size, and hence in duration of afferent conduction, primary P22 activity in the rhesus monkey (Arezzo et al. 1975) compares well with human P30t. Comparisons of later activity seem too speculative.

The present results alone do not allow inferences on the precise location and extent of the structures within the temporal lobe which generate the AEP. Only the primary N19t-P30t component seems to originate unambiguously in a restricted more medially located zone of Heschl's gyri (AI), when considering almost identical correspondence with intracranial records (Celesia 1976). According to our results, the effective electrical centre of the LAEP lies within the auditory cortex. This confirms previous suggestions on the origin of MAEPs (Geisler et al. 1958; Kraus et al. 1982) and LAEP activities (Vaughan and Ritter 1970; Peronnet et al. 1974; Vaughan et al. 1980).

The finding of a secondary (N27r-P39r) middle latency activity, clearly distinct from primary N19t-P30t by an 8 msec difference in latency and by orientation, is new. Although the orientation of this initial radial component is similar to that of neural elements of the paraconiocortical layers

(Galaburda and Sanides 1980), attribution to AII or AAI is not permissible without furher evidence. Even more caution is required in interpretation of the late radial P100r-N150r activity, which compares well with the lateral T complex described by Wolpaw and Penry (1975, 1977). Incidentally, neuromagnetic recordings cannot resolve the sources of these radial components, because of insensitivity to radially oriented dipole activity.

Discussion of contralateral pathway dominance, although clearly evident from our results, is beyond the aim of this paper. Because hemispheric comparisons were based on parameters averaged for right and left ear stimulations, the small effects of contralateral pathway dominance were effectively counterbalanced. Under this condition significant hemispheric differences were not found for dipole strength and amplitude parameters in the normal group. The variability of effective dipole moment in normals should essentially reflect geometrical-anatomical differences of the two hemispheres, if the whole 3-D dipole vector field is considered. In contrast, if peak amplitudes in scalp derivations are compared, additional variability is introduced by the variability of dipole orientation (Fig. 6, cf., cases A and B) and the choice of reference electrode.

Dipole source potentials are reference-free, similar to source derivations (Hjorth 1975) and source density analyses of scalp potentials (MacKay 1984). But our approach is more general, not restricted to the enhancement of radially oriented activity for superficial cortex and, to a great extent, independent of the recording montage. Compared to principal component analysis (Scherg and Von Cramon 1984) it has the advantage of restricting degrees of freedom by constraints based on the physical laws of electrical field propagation in conductive media. Considering the fundamental eqns. 1 and 2, the presented methods can be readily extended to describe 3-dimensional scalp potential distributions by regional sources having 3 orthogonal (or oblique) dipole vector components which account for the 3-dimensional folding of the underlying neuroanatomical substrate. In any case, the number of regional source components which can be derived from an instantaneous scalp distribution is limited by the number of recording channels and by the residual biological noise. Noise effects need to be examined carefully before a decomposition according to a certain source model can be accepted. Stability can be increased by imposing additional temporal constraints using, for example, the spatio-temporal dipole model, which, in the case of the MAEP, allowed for separation of brain-stem and myogenic from temporal lobe activities. The similarity of dipole source potentials obtained from simultaneous 12-channel and 4-channel electrical records may have illustrated the time and cost effective availability of information on the function of a localized neuroanatomical substrate in clinical cases, as compared to the expense actually required for neuromagnetic measurements. According to the methods outlined, any type of event-related potentials may be decomposed into dipole source potentials, provided an approximation in terms of regional, morphologically reasonable sources can be found.

Résumé

Potentiels de source d'un dipôle évoqué sur le cortex auditif de l'homme

Une nouvelle description du potentiel évoqué en termes de 'potentiels de source dipôlaire' est présentée, sur la base de lois physiques liant l'activité électrique intracrâniale et les potentiels de scalp. Enregistrée avec une électrode suffisamment lointaine, l'activité électrique d'une région spatialement restreinte peut être approchée par un champ vectoriel dipôlaire variable dans le temps, avec une localisation stationnaire équivalente. Chacune de ses 3 projections sur un système coordonnées 3-D présente une 'composante source du dipôle' donné. Les amplitudes de ces composantes sont fonctions du temps et appelées 'potentiels de source du dipôle'.

La distribution 2-D coronaire sur le scalp des PEA de latence moyenne et longue obtenue chez 15 sujets normaux, a pu être optimalement décomposée en composantes tangentielle et radiaire du dipôle nées des structures auditives dans les deux lobes temporaux. L'activité tangentielle initiale

(N19t-P30t) a semblé provenir du cortex auditif primaire et l'activité radiaire initiale (N27r-P39r) du cortex auditif secondaire, étant donné la similarité avec les enregistrements intracrâniaux (Celesia 1976). Les lésions unilatérales des radiations acoustiques ont aboli les potentiels de source du dipôle PEAM ipsilatéral. Des lésions impliquant AI/II et AAI ont également aboli les potentiels de source PEAL dans l'hémisphère atteint. Les potentiels de source du dipôle normal dans l'hémisphère intact suffisaient à expliquer les distributions sur le scalp chez ces patients. En cas d'interruption probable des entrées corticales primaires, la présence de potentiels de source d'un dipôle tardif, lequel était retardé de 20 à 30 msec, reflétait probablement une activation corticale par l'intermédiaire des fibres commissurales.

We wish to thank A. Geigenberger, B. Steidle and G. Stenglein for their great help in obtaining the recordings.

References

Arezzo, J., Pickoff, A. and Vaughan, Jr., H.G. The sources and intracerebral distribution of auditory evoked potentials in the alert rhesus monkey. Brain Res., 1975, 90: 57–73.

Brinkmann, R.D. and Scherg, M. Human auditory on- and off-potentials of the brainstem. Scand. Audiol., 1979, 8: 27–32.

Celesia, G.G. Organization of auditory cortical areas in man. Brain, 1976, 99: 403–414.

Cohen, M.M. Coronal topography of the middle latency auditory evoked potentials (MLAEPs) in man. Electroenceph. clin. Neurophysiol., 1982, 53: 231–236.

Davis, P.A. Effects of acoustic stimuli on the waking human brain. J. Neurophysiol., 1939, 2: 494–499.

Farrell, D.E., Tripp, J.H., Norgren, R. and Teyler, T.J. A study of the auditory evoked magnetic field of the human brain. Electroenceph. clin. Neurophysiol., 1980, 49: 31–37.

Galaburda, A. and Sanides, F. Cytoarchitectonic organization of the human auditory cortex. J. comp. Neurol., 1980, 190: 597–610.

Geisler, C.D., Frishkopf, L.S. and Rosenblith, W.A. Extracranial responses to acoustic clicks in man. Science, 1958, 128: 1210–1211.

Gerull, G., Giesen, M., Knüpling, R. und Mrowinski, D. Hörbahnuntersuchung mit akustisch evozierten Hirnpotentialen mittlerer Latenz. Laryng.-Rhinol., 1981, 60: 135–138.

Goff, G.D., Matsumiya, Y., Allison, T. and Goff, W.R. The scalp topography of human somatosensory and auditory evoked potentials. Electroenceph. clin. Neurophysiol., 1977, 42: 57–76.

Hari, R., Aittoniemi, K., Jaervinen, M.-L., Katila, T. and Varpula, T. Auditory evoked transient and sustained magnetic fields of the human brain. Exp. Brain Res., 1980, 40: 237–240.

Hjorth, B. An on-line transformation of EEG scalp potentials into orthogonal source derivations. Electroenceph. clin. Neurophysiol., 1975, 39: 526–530.

Jerger, J., Weikers, N.J., Sharbrough, III, F.W. and Jerger, S. Bilateral lesions of the temporal lobe. Acta oto-laryng. (Stockh.), 1969, Suppl. 258: 7–51.

Knight, R.T., Hillyard, S.A., Woods, D.L. and Neville, H.J. The effects of frontal and temporal-parietal lesions on the auditory evoked potential in man. Electroenceph. clin. Neurophysiol., 1980, 50: 112–124.

Kooi, K.A., Tipton, A.C. and Marshall, R.E. Polarities and field configurations of the vertex components of the human auditory evoked response: a reinterpretation. Electroenceph. clin. Neurophysiol., 1971, 31: 166–169.

Kraus, N., Özdamar, Ö., Hier, D. and Stein, L. Auditory middle latency responses (MLRs) in patients with cortical lesions. Electroenceph. clin. Neurophysiol., 1982, 54: 275–287.

MacKay, D.M. Source density analysis of scalp potentials during evaluated action. I. Coronal distribution. Exp. Brain Res., 1984, 54: 73–85.

McCallum, W.C. Some sensory and cognitive aspects of ERPs: a review. In: H.H. Kornhuber and L. Deecke (Eds.), Motivation, Motor, and Sensory Processes of the Brain. Prog. in Brain Res., Vol. 54. Elsevier, Amsterdam, 1980: 261–278.

McCallum, W.C. and Curry, S.H. Hemisphere differences in event related potentials and CNVs associated with monaural stimuli and lateralized motor responses. In: D. Lehmann and E. Callaway (Eds.), Human Evoked Potentials. Plenum Press, New York, 1979: 235–250.

Michel, F. et Peronnet, F. L'hémianacousie, un déficit auditif dans un hémisphère. Rev. neurol., 1982, 138: 657–671.

Michel, F., Peronnet, F. and Schott, B. A case of cortical deafness: clinical and electrophysiological data. Brain Lang., 1980, 10: 367–377.

Özdamar, Ö., Kraus, N. and Curry, F. Auditory brain stem and middle latency responses in a patient with cortical deafness. Electroenceph. clin. Neurophysiol., 1982, 53: 224–230.

Pandya, D.N. and Seltzer, B. Association areas of the cerebral cortex. Trends Neurosci., 1982, 5: 286–390.

Parving, A., Salomon, G., Elberling, C., Larsen, B. and Lassen, N.A. Middle components of the auditory evoked response in bilateral temporal lobe lesions. Scand. Audiol., 1980, 9: 161–167.

Peronnet, F., Michel, F., Echallier, J.F. and Girod, J. Coronal topography of human auditory evoked responses. Electroenceph. clin. Neurophysiol., 1974, 37: 225–230.

Perrault, N. and Picton, T.W. Event-related potentials recorded from the scalp and nasopharynx. I. N1 and P2. Electroenceph. clin. Neurophysiol., 1984, 59: 177–194.

Picton, T.W., Hillyard, S.A., Krausz, H.I. and Galambos, R. Human auditory evoked potentials. I. Evaluation of com-

ponents. Electroenceph. clin. Neurophysiol., 1974, 36: 179–190.

Polich, J.M. and Starr, A. Middle-, late-, and long-latency auditory evoked potentials. In: E.J. Moore (Ed.), Bases of Auditory Brain-Stem Evoked Responses. Grune and Stratton, New York, 1983: 345–361.

Romani, G.L., Williamson, S.J., Kaufman, L. and Brenner, D. Characterization of the auditory cortex by the neuromagnetic method. Exp. Brain Res., 1982, 47: 381–393.

Scherg, M. Distortion of the middle latency auditory response produced by analog filtering. Scand. Audiol., 1982a, 11: 57–60.

Scherg, M. Simultaneous recording and separation of early and middle latency auditory evoked potentials. Electroenceph. clin. Neurophysiol., 1982b, 54: 339–341.

Scherg, M. Räumlich-zeitliche Analyse der akustisch evozierten Potentiale mittlerer Latenz. NTZ Arch., 1984a, 6: 287–291.

Scherg, M. Spatio-temporal modelling of early auditory evoked potentials. Rev. Laryng. (Bordeaux), 1984b, 105: 163–170.

Scherg, M. and Von Cramon, D. Topographical analysis of auditory evoked potentials: derivation of components. In: R.H. Nodar and C. Barber (Eds.), Evoked Potentials, II. Butterworth, Woburn, 1984: 73–81.

Scherg, M. and Von Cramon, D. Two bilateral sources of the late AEP as identified by a spatio-temporal dipole model. Electroenceph. clin. Neurophysiol., 1985a, 62: 32–44.

Scherg, M. and Von Cramon, D. A new interpretation of the generators of BAEP waves I–V: results of a spatio-temporal dipole model. Electroenceph. clin. Neurophysiol., 1985b, 62: 290–299.

Scherg, M. and Von Cramon, D. Psychoacoustic and electrophysiologic correlates of central hearing disorders in man. Europ. Arch. psychiat. neurol. Sci., 1986, in press.

Vaughan, Jr., H.G. The neural origins of human event-related potentials. In: I. Bodis-Wollner (Ed.), Evoked Potentials. Ann. N.Y. Acad. Sci., 1982, 388: 125–138.

Vaughan, Jr., H.G. and Ritter, W. The sources of auditory evoked responses recorded from the human scalp. Electroenceph. clin. Neurophysiol., 1970, 28: 360–367.

Vaughan, Jr., H.G., Ritter, W. and Simson, R. Topographic analysis of auditory event-related potentials. In: H.H. Kornhuber and L. Deecke (Eds.), Motivation, Motor, and Sensory Processes of the Brain. Prog. in Brain Res., Vol. 54, Elsevier, Amsterdam, 1980: 279–285.

Wolpaw, J.R. and Penry, J.K. A temporal component of the auditory evoked response. Electroenceph. clin. Neurophysiol., 1975, 39: 609–620.

Wolpaw, J.R. and Penry, J.K. Hemispheric differences in the auditory evoked response. Electroenceph. clin. Neurophysiol., 1977, 43: 99–102.

Wolpaw, J.R. and Wood, C.C. Scalp distribution of human auditory evoked potentials. I. Evaluation of reference electrode sites. Electroenceph. clin. Neurophysiol., 1982, 54: 15–24.

Wood, C.C. and Wolpaw, J.R. Scalp distribution of human auditory evoked potentials. II. Evidence for overlapping sources and involvement of auditory cortex. Electroenceph. clin. Neurophysiol., 1982, 54: 25–38.

Wood, C.C., McCarthy, G., Squires, N.K., Vaughan, H.G., Woods, D.L. and McCallum, W.C. Anatomical and physiological substrates of event-related potentials. In: R. Karrer, J. Cohen and P. Tueting (Eds.), Brain and Information: Event-Related Potentials. Ann. N.Y. Acad. Sci., 1984, 425: 681–721.

Woods, D.L., Knight, R.T. and Neville, H.J. Bitemporal lesions dissociate auditory evoked potentials and perception. Electroenceph. clin. Neurophysiol., 1984, 57: 208–220.